ELSEVIER   PII: S0141-1187(97)00015-1

Near-trapping of waves by circular arrays of vertical cylinders

D.V. Evans & R. Porter

School of Mathematics, University of Bristol, Bristol BS8 1TW, UK

The effect of incident waves on arrays of identical bottom-mounted circular cylinders arranged in a circle are considered. The present paper is motivated by the recent work of Maniar and Newman [Maniar, H.D. and Newman, J.N., *Journal of Fluid Mechanics*, 1997, **339**, 309–330], who show how large forces can be generated on long linear arrays at certain frequencies corresponding to trapped modes present in an infinite periodic linear array. Their analysis for the linear array motivates the idea of 'near trapping' in circular arrays in which it is assumed that adjacent cylinders only differ by a change in phase characterised by an integer, *p*. By using the interaction theory of Linton and Evans [Linton, C.M. and Evans, D.V., *Journal of Fluid Mechanics*, 1990, **215**, 549–569] it is shown how large peaks in the forces on circular arrays of four, five and six cylinders develop as the gap between the cylinders is reduced, and the peaks are shown to correspond to particular values of *p* by examining the complex roots of the near-trapping system. The largest forces appear to arise when the near-trapped mode corresponds to a standing wave motion, in agreement with the largest forces in linear arrays. © 1997 Elsevier Science Limited

1 INTRODUCTION

The effect of ocean waves on the supporting columns of an offshore structure is clearly of fundamental importance in design considerations and numerous papers have been written exploring the possibility that the waves scattered by the columns could constructively interfere, causing large exciting wave loads or drift forces in certain circumstances. The simplest configuration, that of an array of bottom-mounted cylinders of circular cross-section, has received most attention since, apart from its applicability to the supports of an oil-drilling platform, it also models the scattering of a plane acoustic wave in two dimensions by an array of 'hard' cylinders, once the depth dependence has been removed. In this context the most notable early work was that of Twersky [1], who constructed a solution for the scattered field by using an iterative procedure in which the successive scattering by each cylinder was introduced at each order to produce an infinite series of orders of 'scattering'. Ohkusu [2] applied Twersky's method in the context of water waves rather than acoustics whilst Spring and Monkmeyer [3] utilised a direct method to obtain the first-order exciting forces on elements of the array by applying the boundary condition on all cylinders simultaneously.

Linton and Evans [4] improved upon this and provided simple expressions for the first-order exciting forces and mean drift forces in terms of the coefficients of an infinite system of equations. This formulation has recently been used by Huang and Eatock-Taylor [5] to solve for the full second-order diffraction potential. For more complicated arrays of axisymmetric bodies the method of Twersky has been adopted by Mavrakos and Koumoutsakos [6], whilst a general approach applicable to any array in which the diffraction characteristics of each of the individual elements is known has been developed by Kagemoto and Yue [7].

The present paper is motivated by recent work of Maniar and Newman [8] on the first-order exciting forces on a large number of identical, equally spaced, bottom-mounted circular cylinders in a line. They showed that at an incident wave frequency close to that of a trapped mode, which arises in the case of a cylinder on the centre-plane of a channel, large forces are experienced by those cylinders near the centre of the array. The existence of such trapped modes was first proved by Callan *et al.* [9] using a method developed by Ursell [10] in proving existence in the case of a totally submerged, infinitely long *horizontal* cylinder. Callan *et al.* [9] showed that the modes, which are antisymmetric with respect to the mid-plane of the channel and satisfy the
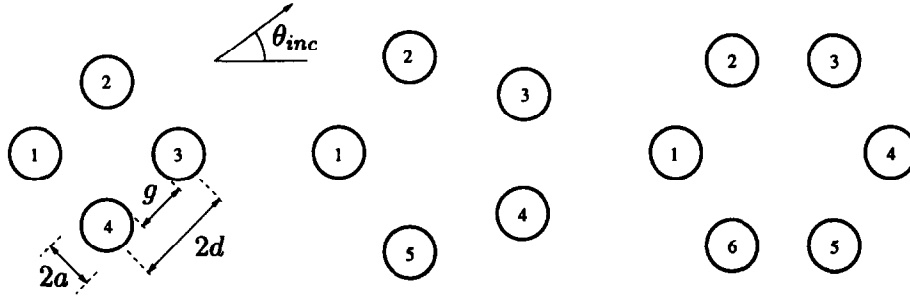
Fig. 1. Arrangement, dimensions and cylinder labels for circular arrays of four, five and six cylinders.

condition of no flow through the channel walls, occur at a unique wavenumber for all sizes of cylinder. Experimental confirmation of these modes has recently been provided by Retzler (private communication). Subsequently, theoretical results of Evans et al. [11] and Davies and Parnovski [12] have shown the existence of such trapped modes for a wide range of cylinder cross-sections. Maniar and Newman [8] show that as the number of cylinders in the linear array increases, the force on the cylinders near the centre of the array also increases for a frequency close to the trapped-mode frequency since the array more closely resembles an infinite array which is equivalent through reflections in the channel walls to the trapped-mode situation. However, Maniar and Newman [8] also obtained large forces at a frequency corresponding to what they term Dirichlet trapped modes. These are trapped modes which have no physical interpretation in the water-wave context but which have been predicted and confirmed experimentally in acoustics; see, for example, Parker and Stoneman [13] for an extensive review. The Dirichlet modes have the property that they vanish on the sides of the channel or, equivalently, on each mid-plane between adjacent cylinders in an infinite periodic array.

The large forces experienced by cylinders in a finite array are a consequence of what we shall term near-trapping. By this we mean a local oscillation in the vicinity of the array at a well-defined frequency which decays slowly as its energy leaks away due to wave radiation at large distances.

Prompted by these results for large but finite linear arrays of identical bottom-mounted cylinders, we decided to look at the familiar and important case of a circular array of N equally spaced, identical, bottom-mounted cylinders to see if large forces corresponding to near-trapping could occur here also. The case for $N = 4$ and 5 has clear relevance to the supporting columns of an offshore drilling platform. The method employed is that used by Linton and Evans [4], which they applied to precisely this problem but without the possibility of near-trapping in mind. Our initial investigations were for large N since we expected, by analogy with the finite linear array, that this was necessary to obtain near-trapping. In fact, this proves not to be the case. We find that near-trapping occurs for N as small as four and that as N increases, the exciting force on each cylinder shows rapid variations at particular frequencies and spacings between cylinders. Because of their important applicability we

shall concentrate in the present paper on interpreting our results for $N = 4$, 5 and 6. We shall make use of the general formulation of Linton and Evans [4] which is given in Appendix A.

In Section 2 we discuss the results for the exciting force and mean second-order drift forces on configurations of four, five and six cylinders arranged in a circle and show how extremely large forces can indeed occur at certain spacings and wave frequencies. We seek near-trapping solutions directly by dropping the incident wave-field and making assumptions about the phase factors between neighbouring cylinders. The ideas developed by Maniar and Newman [8] for linear arrays are applied to the circular array, notably in dictating the choice of the integer p, which relates the difference in phase between adjacent cylinders in the circular array, for predicting the large forces and motions. The results are discussed in Section 3 where free-surface plots are used to explain the occurrence of the large forces on cylinders in circular arrays at frequencies corresponding to near-trapping.

2 FORCES ON CIRCULAR ARRAYS OF IDENTICAL CYLINDERS

In this section we shall be concerned with the forces on circular arrays of four, five and six cylinders arranged as shown in Fig. 1. For simplicity we shall only consider an incident wave progressing in the positive x-direction ($\theta_{inc} = 0$) such that the cylinder labelled as 1 is the lead cylinder and so that the results for the forces are symmetrical. Note that this labelling is different from that used in Fig. 25 and throughout the rest of the paper in developing the analysis. The cylinders have diameter $2a$ with $2d$ being the distance between adjacent cylinders. It is illuminating to define a gap-to-diameter ratio, $g/2a = d/a - 1$, being the ratio of the gap between adjacent cylinders to a cylinder diameter. The circled numbers against the peaks in the curves that follow will be referred to later in the paper. The results are derived by computing eqns (A.20) and (A.23) using B_n calculated from eqn (A.16).

Results for the total maximum force on each of the four cylinders in a circular array with $\theta_{inc} = 0$ against the non-dimensional wavenumber κa as the ratio a/d varies are presented in Figs 2a–e. In Fig. 2a, $a/d = 0.5$ as in Linton and
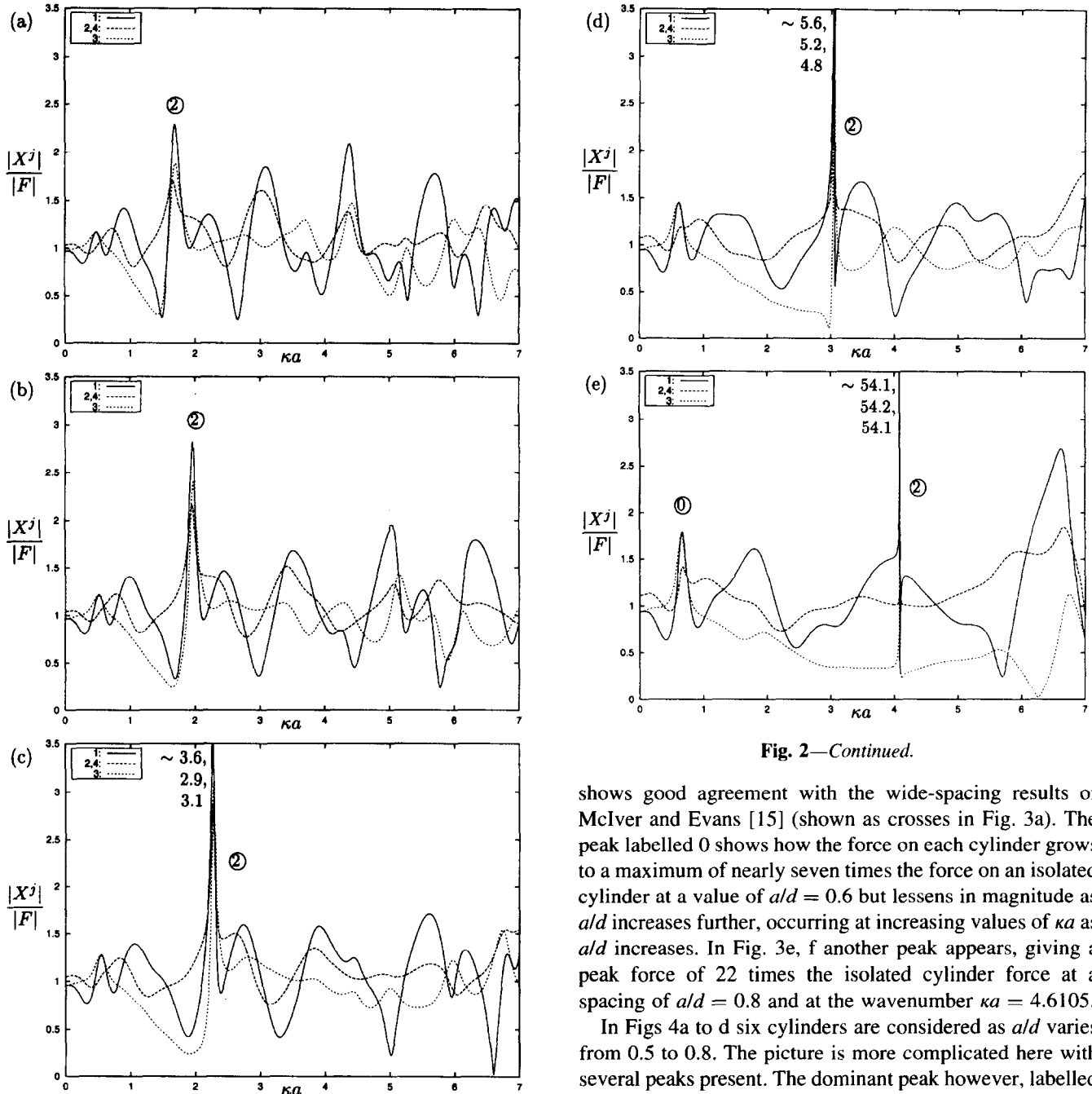
Fig. 2. Resultant force on four cylinders against wavenumber, κa: $\theta_{inc} = 0$, $a/d = 0.5$ (a), 0.55 (b), 0.6 (c), 0.7 (d), 0.8 (e).

Fig. 2—*Continued.*

Evans [14]. Notice the peak in the force on each cylinder at roughly the same value of $\kappa a \approx 1.66$. Figures 2b to e show the effect of bringing the cylinders closer together and it can be seen that the peaks increase markedly as a/d increases (or $g/2a$ decreases) to such an extent that for $a/d = 0.8$ ($g/2a = 0.25$) in Fig. 2e the peak force on *all four* cylinders is some 54 times the force on an isolated cylinder. This can only be due to a near-trapped wave at the wavenumber given by $\kappa a = 4.08482$.

The sequence of Figs 3a–f repeats the process for five cylinders starting with a spacing ratio of $a/d = 0.4$ and

shows good agreement with the wide-spacing results of McIver and Evans [15] (shown as crosses in Fig. 3a). The peak labelled 0 shows how the force on each cylinder grows to a maximum of nearly seven times the force on an isolated cylinder at a value of $a/d = 0.6$ but lessens in magnitude as a/d increases further, occurring at increasing values of κa as a/d increases. In Fig. 3e, f another peak appears, giving a peak force of 22 times the isolated cylinder force at a spacing of $a/d = 0.8$ and at the wavenumber $\kappa a = 4.6105$.

In Figs 4a to d six cylinders are considered as a/d varies from 0.5 to 0.8. The picture is more complicated here with several peaks present. The dominant peak however, labelled by a circled 3, rises to a value of 225 times the force on a single cylinder in isolation, again for all six cylinders, for a spacing of $a/d = 0.8$ and a wavenumber $\kappa a = 2.92921$. It is clear that this frequency also corresponds to a near-trapped mode.

By using eqns (A.23), (A.24) we can also compute the mean second-order drift force in radial and tangential directions on all of the cylinders in the array. Rather than show curves of these, which are not particularly interesting apart from at the near-trapping frequencies, we only present, in Table 1, maximum drift forces attained at these frequencies for the most extreme case considered in the first-order force plots of $a/d = 0.8$.

The total drift force on the cylinder array as a whole, however, does not experience a peak as the wavenumber
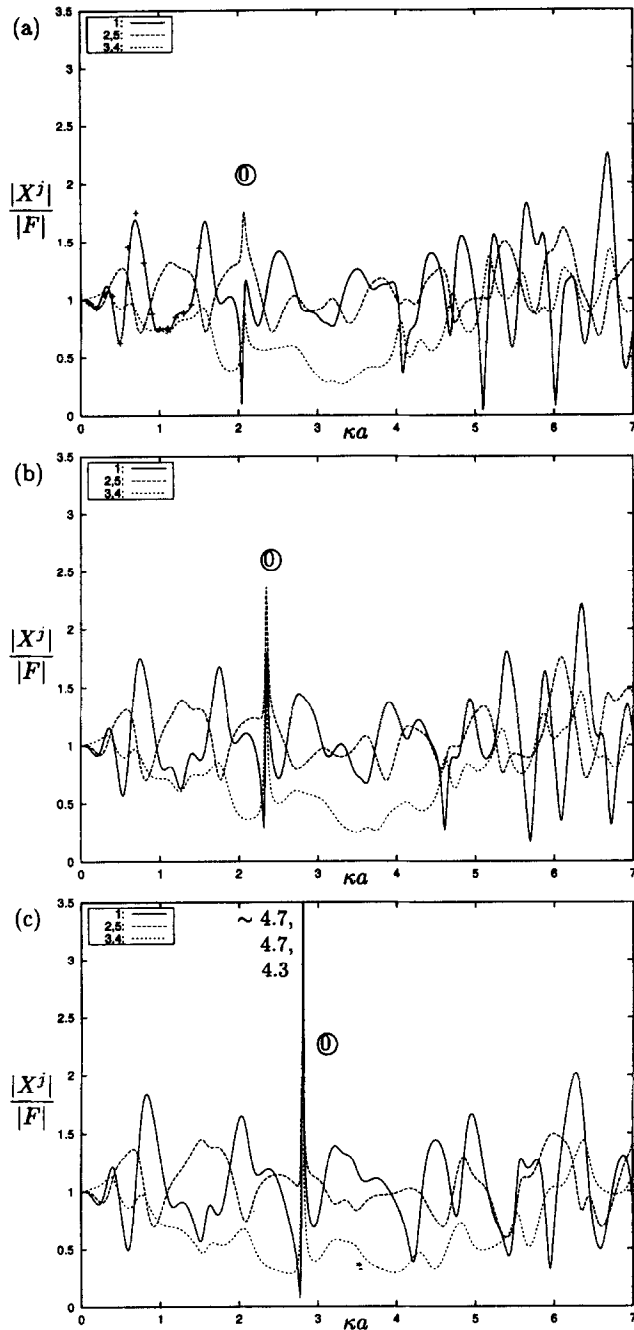
Fig. 3. Resultant force on five cylinders against wavenumber, κa:
$\theta_{inc} = 0$, $a/d = 0.4$ (a), 0.45 (b), 0.5 (c), 0.6 (d), 0.7 (e), 0.8 (f).

Fig. 3—*Continued.*

passes through the resonant wavenumber due to cancellation from the individual elements of the array. The values for the peak drift force in Table 1 seem to be related roughly to the square of the corresponding peak forces from Figs 2e, 3f and Fig. 4d.

We shall see later that these large forces are accompanied by large motions in the vicinity of the cylinders. In a sense this is to be expected since as the gap ratio $g/2a$ decreases the enclosed water region resembles more closely a harbour with a narrow entrance and large motions can be expected at frequencies close to the 'resonant' frequencies of the internal fluid region. This is confirmed in Fig. 5 which
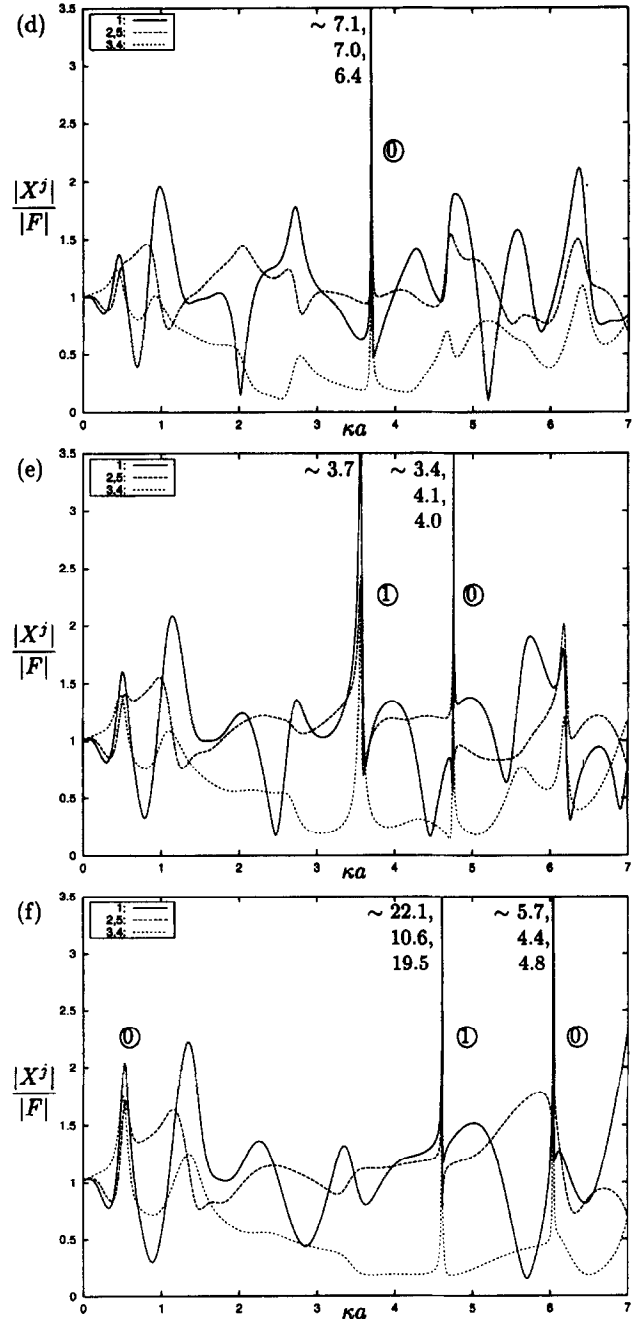
plots, for four cylinders, the maximum force on the lead cylinder against the gap ratio, and shows how the force increases with decreasing $g/2a$. One has to take care when numerically computing the forces for $g/2a$ smaller than 0.2, since a larger truncation parameter is needed in the infinite system of equations. That the large force is not simply a narrow entrance harbour effect can be seen from Fig. 6, where the forces on four cylinders with $a/d = 0.8$ are computed when the diameter of one of the cylinders is increased by just 2%. Despite the narrowing of the gap between it and its neighbours we see by comparison with Fig. 2e that the maximum force is reduced to less than 4.5 once the symmetry has been broken.
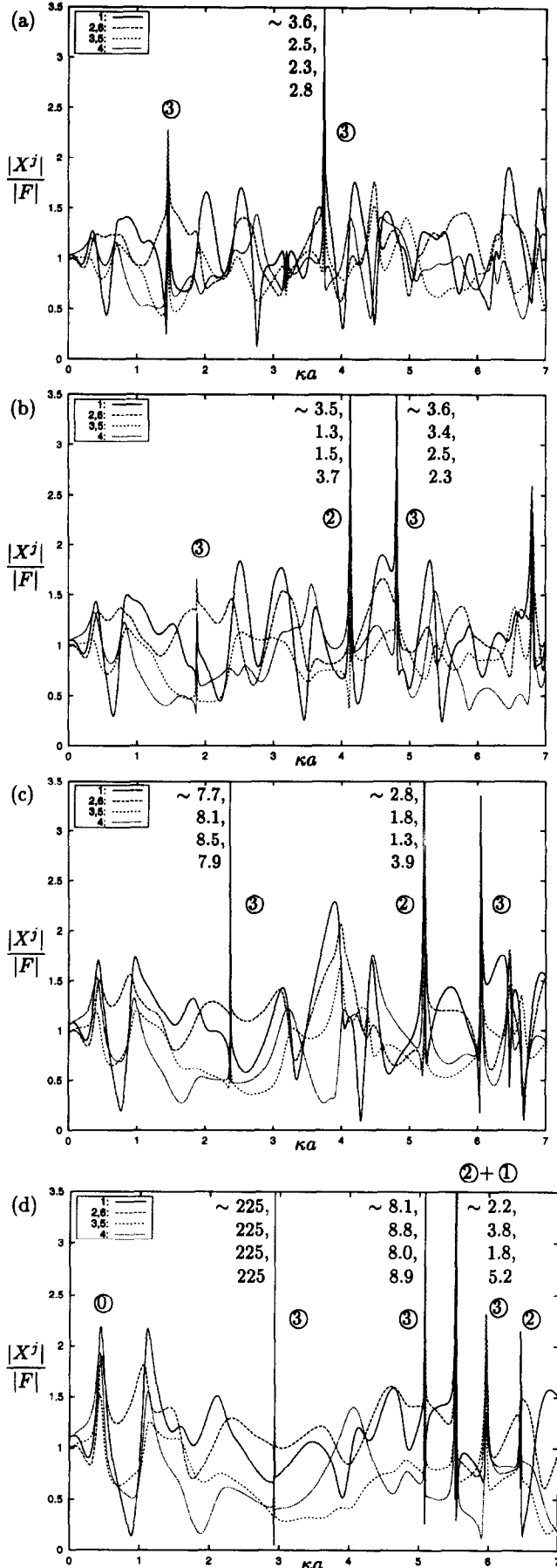
Table 1. Modulus of mean second-order drift forces in the three resonant cases for $N = 4,5,6$ with $\theta_{inc} = 0$, $a/d = 0.8$

	Cylinder number		
	1	2,4	3
$N = 4$ $\kappa a = 4.08482$	2384	2393	2364
	Cylinder number		
	1	2,5	3,4
$N = 5$ $\kappa a = 4.6105$	341	123	265
	Cylinder number			
	1	2,6	3,5	6
$N = 6$ $\kappa a = 2.92922$	45 807	45 833	45 815	45 627

It is clear that the large forces and amplitudes of motion in the vicinity of the cylinders at frequencies and spacings corresponding to near-trapping are related to the near-vanishing of the determinant of the infinite system [eqn (A.16)]. It is clear that this determinant is independent of the incident wave, which only appears on the right-hand side of eqn (A.16), and that a more direct approach to near-trapping is to assume that the B_n^j are related purely through a phase factor describing the angle between cylinder k and cylinder j. A similar assumption was made by Maniar and Newman [8] in considering the long linear array. The result of this assumption is shown in Appendix A, eqn (A.24), to reduce the infinite system to the simpler single infinite system, eqn (A.25), with K_{mn} given by eqn (A.28). Different choices of p give rise to different radial and tangential phase relationships between forces on adjacent cylinders but we can make progress for general p as follows. Thus, from eqn (A.26), we first replace the summation variable, j, by $-j$ and then substitute, without loss of generality, the value of $k = 1$ to give

$$K_{-m,\,-n}(p) = Z_n^0 \sum_{j=1}^{N-1} H_{n-m}\left(2\kappa R \sin \frac{\pi j}{N}\right)$$

$$\times e^{i\frac{1}{2}(n-n)\pi} e^{i(n+m+2p)\pi j/N} \tag{1}$$

in an obvious notation, but different to that used in eqn (A.27), and comparison with eqn (A.28) gives us

$$K_{-m,\,-n}(p) = (-1)^{n-m} K_{mn}(N-p) \tag{2}$$

whilst it is clear from eqn (A.28) that

$$K_{mn}(0) = K_{mn}(N) \tag{3}$$

It follows from using eqn (2) in eqn (A.25) that $(-1)^m B^0_{-m}(N-p)$ satisfies the same homogeneous

Fig. 4. Resultant force on six cylinders against wavenumber, κa: $\theta_{inc} = 0$, $a/d = 0.5$ (a), 0.6 (b), 0.7 (c), 0.8 (d).
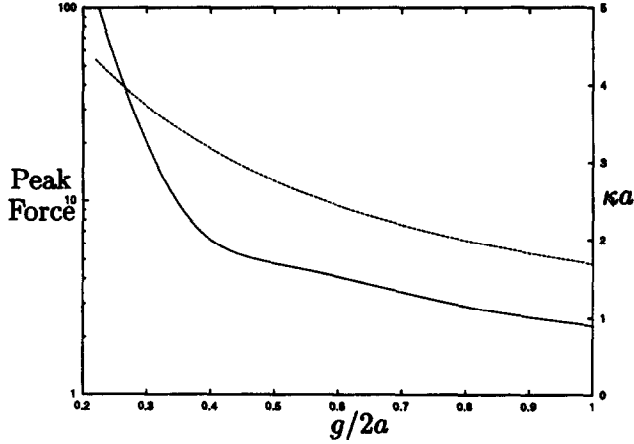
Fig. 5. The variation of non-dimensional peak force (——, left scale) and wavenumber κa at which it occurs (- - -, right scale) on the lead cylinder in acircular array, $N = 4$ ($\theta_{\mathrm{inc}} = 0$), as the gap ratio $g/2a$ varies.

equation as $B_m^0(p)$ and that the two systems share the same determinant. This immediately gives us that the values of κd at which the determinant vanishes for a particular value of p are the same as those for $N - p$. Moreover

$$B_m^0(p) = C(-1)^m B_{-m}^0(N-p)$$

and so

$$B_m^0(N-p) = C(-1)^m B_{-m}^0(p) \qquad (4)$$

which implies that $C^2 = 1$ or $C = \pm 1$. In particular, choosing $p = N/2$, N even, gives

$$B_m^0(N/2) = \pm (-1)^m B_{-m}^0(N/2) \qquad (5)$$

We can also use the information in eqn (3) to deduce from eqn (A.25) that $B_m^0(0) = CB_m^0(N)$, which, when used in eqn (4) with $p = 0$, gives

$$B_m^0(0) = C(-1)^m B_0^0(0) \qquad (6)$$

It remains for us to look at the radial and tangential forces due to these two modes of resonance. Thus from eqn (A.20)
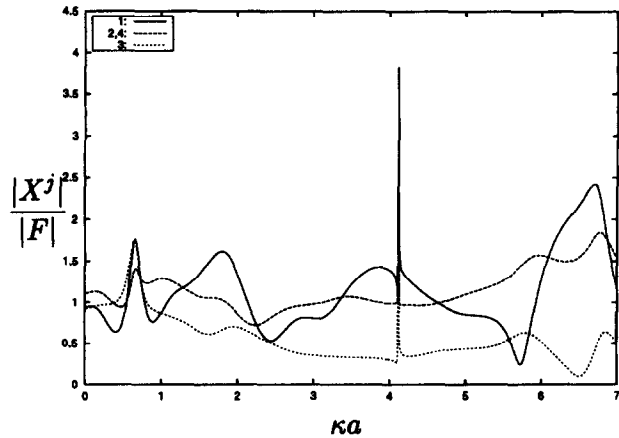

Fig. 6. Resultant force on unsymmetric arrangement of four cylinders against wavenumber, κa: $\theta_{\mathrm{inc}} = 0$, $a_1/d = 0.82$, $a_i/d = 0.8$, $i = 2,3,4$.

with $p = N/2$ in eqn (A.24) to relate cylinder j to cylinder 0

$$X_r^j(N/2) = -\frac{1}{2}i(-1)^j\left(B_{-1}^0(N/2) - B_1^0(N/2)\right)$$

$$= \begin{cases} i(-1)^j B_1^0(N/2), & C = 1 \\ 0, & C = -1 \end{cases} \qquad (7)$$

$$X_r^j(N/2) = -\frac{1}{2}(-1)^j\left(B_{-1}^0(N/2) + B_1^0(N/2)\right)$$

$$= \begin{cases} 0, & C = 1 \\ -(-1)^j B_1^0(N/2), & C = -1 \end{cases} \qquad (8)$$

In other words, the force is either radial or tangential, but never a combination of the two, and switches in sign from one cylinder to the next. Likewise, with $p = 0$ (or N)

$$X_r^j(0) = -\frac{1}{2}i\left(B_{-1}^0(0) - B_1^0(0)\right)$$

$$= \begin{cases} iB_0^j(0), & C = 1 \\ 0, & C = -1 \end{cases} \qquad (9)$$

$$X_r^j(0) = -\frac{1}{2}\left(B_{-1}^0(0) + B_1^0(0)\right)$$

$$= \begin{cases} 0, & C = 1 \\ -B_1^0(0), & C = -1 \end{cases} \qquad (10)$$

giving the previous result; namely that the force can only ever be either totally radial or totally tangential, but here the sense in which the force acts is the same for all the cylinders in the array. This mode therefore corresponds to either a tangential torque on the array or a radial pull on the array. These four cases are illustrated in Fig. 7. For other values of p, there does not appear to be a simple way of predicting the direction of the force on the cylinders in the array.

The four possible resonant modes summarised in Fig. 7 can each be shown to possess symmetries of motion about lines joining the centre of the array to the centres of the cylinders and those from the centre passing midway between adjacent cylinders. For example, in case (a)(i) in Fig. 7, from the expression for the potential close to cylinder k

$$\frac{\partial \phi(r_k, 0)}{\partial \theta} = \frac{\partial}{\partial \theta} \sum_{n=-\infty}^{\infty} B_n^k F_n(\kappa r_k)\, e^{in\theta_k}\Bigg|_{\theta_k = 0} \qquad (11)$$
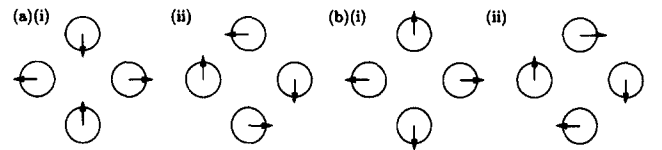

Fig. 7. An illustration of the two possible forces in the resonant modes corresponding to (a) $p = N/2$, (b) $p = 0, N$.

where $F_n = (-1)^n F_{-n}$ is defined in eqn (A.11). Then

$$\frac{\partial\phi(r_k,0)}{\partial\theta} = \frac{\partial}{\partial\theta} \sum_{n=-\infty}^{\infty} in B_n^k F_n$$

$$= (-1)^k \frac{i}{2} \sum_{n=\infty}^{\infty} n F_n \left(B_n^0(N/2)\right)$$

$$- (-1)^n B_{-n}^0(N/2)) \tag{12}$$

since $p = N/2$,

$$= 0, \text{ for } C = 1, \text{ or case (a)(i)} \tag{13}$$

and therefore there is symmetry about the lines joining the centre of the array to the centres of the cylinders. Similarly, it is trivial to show that there is antisymmetry about the lines passes midway between adjacent cylinders in this case.

It appears from our computations that all four near-trapped mode types associated with $p = 0$, $N/2$ and illustrated in Fig. 7 exist, and this can be seen more clearly by looking at the free-surface plots.

3 RESULTS FOR CIRCULAR ARRAYS OF FOUR, FIVE AND SIX CYLINDERS

In order to assist our understanding of the various resonant motions due to near-trapping that have become apparent in the force plots, and whose frequencies can be predicted from the determinant system [eqn (A.25)], we shall also use free-surface plots. The elevation of the free surface, $H(x,y,t) = \text{Re}\{\eta(x,y) e^{-i\omega t}\}$, non-dimensionalised with respect to an incident wave of unit amplitude, is given by

$$\eta(x, y) = \phi(x, y)$$

In all the free-surface plots presented in this paper, we shall use two plots: one showing $\text{Re}\{\phi\}$, the other $|\phi|$. The former of these two corresponds to the free-surface elevation at a particular instant in time during the cycle, namely at $t = n\pi/\omega$, $n = 0,1,...$ [this can be seen by considering equation eqn (A.1)], and allows us to observe the relative position of peaks and troughs. Alternatively, we could have presented plots of $\text{Im}\{\phi\}$ which corresponds to the free-surface elevation at $t = (n + 1/2)\pi/\omega$, $n = 0,1,....$ Instead, we choose to plot $|\phi|$, which corresponds the maximum free-surface elevation attained over a cycle. The circular array of cylinders are arranged as in Fig. 1 in such a way that the distance between consecutive centres is unity ($2d = 1$), and attention is focused on the interior domain, since the motion outside the array is relatively insignificant and of little interest. Also, since it is near-trapped resonant modes that we seek, we plot the free surface due to the scattered potential only by discarding the influence of the incident wave rather than by using the total potential. In the vicinity of cylinder j, say, we may use the computationally efficient method of calculating the potential given by the expression in eqn (A.11).

Before going any further, it is reasonable to ask whether the assumption for a near-trapped mode given in eqn (A.24) provides all the possible resonances. Numerical experiments performed on a range of array sizes and wave parameters suggest that no others exist. In other words, all resonances correspond to a value of p in the determinant system, eqns (A.25), (A.28), which has assumed eqn (A.24) expressing only a change in phase from one cylinder to the next for the occurrence of a near-trapped mode. An alternative approach would be to appeal to symmetries of the problem as was done by Gaspard and Rice [16] in their consideration of the resonances of a three-disc system on which a 'soft' condition was applied.

It is the determinant system, eqn (A.25), that we turn our attention to next. Given that all resonances are accounted for by a value of p, the determinant system provides a far more efficient way of locating the frequency at which near-trapped modes occur. Not only this, but we can also identify, by means of the value of p, the behaviour of the type of mode. The reader is reminded that choosing $N - p$ gives the same results as choosing p [this comes from eqn (2)] and so we need only restrict ourselves to considering values of $p \leq [N/2]$.

For the purpose of locating the frequency at which a near-trapped mode occurs, and hence where we may expect to find large first- and second-order forces acting on the array, it is sufficient to scan through the non-dimensional wavenumber, κa, as a real parameter and monitor the modulus of the value of the complex determinant. Then whenever the modulus of the determinant dips close to zero, one would expect to find a resonant motion in the forcing problem. But it is perhaps more enlightening to seek the precise zeros of the determinant by regarding κa as a complex variable. This extra dimension adds to the computational effort in locating trapped modes, requiring the use of Newton's method in two dimensions, but in essence is straightforward.

In eqn (A.1) we assumed the decomposition $\Phi(x,y,z,t) = \text{Re}\{\phi(x,y) \cosh \kappa(z + h) e^{-i\omega t}\}$, where $\text{Re}\{\omega\} > 0$ has been assumed throughout in order to satisfy the radiation condition and we must choose $\omega_i \equiv \text{Im}\{\omega\} \leq 0$ to avoid exponential growth of the potential with increasing time. Then it is straightforward to show, by using eqn (A.2), that $\omega_i \leq 0$ then $\kappa_i \equiv \text{Im}\{\kappa\} \leq 0$. If $\kappa_i = 0$, then $\omega_i = 0$ and so the motion is harmonic with no decay in time. That is, a genuine trapped mode. If κ_i is negative, then there is exponential decay in time and the mode is only near-trapped. Of course, the more negative κ_i, the faster decay of an initial resonant disturbance.

The zeros of the complex determinant in the cylinder array are found in the following way. For each value of p, we perform a search of the complex κa space close to the real line for a value of $a/d = 0.8$ using Newton's method and pick out the complex values of κa corresponding to a zero of the determinant in this region. For each of these values a/d is then varied from 0.8 to 0.5 in small steps, so as to trace the path of the zero as the
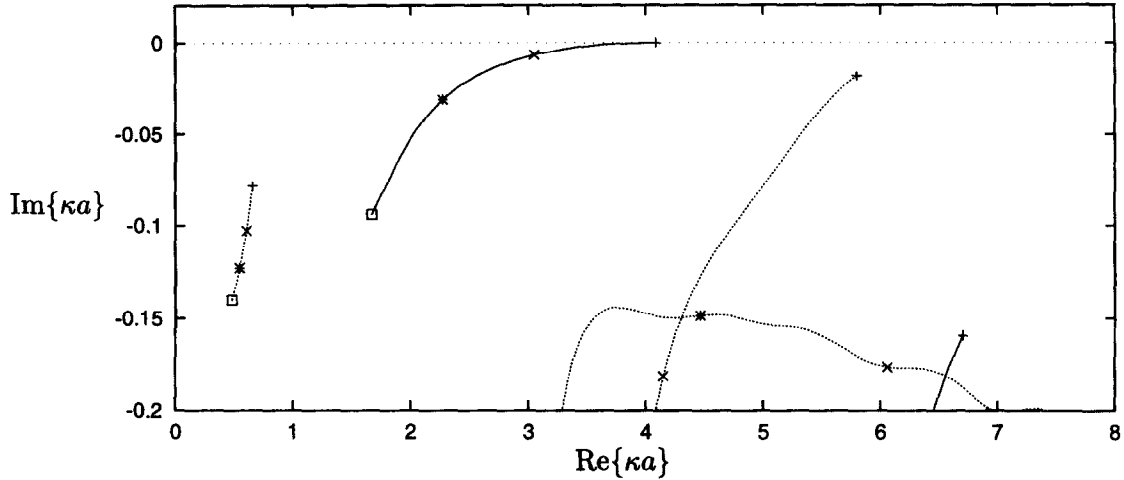
D. V. Evans, R. Porter

Fig. 8. Location of zeros of determinant in complex wavenumber κa space for $N = 4$ cylinders as a/d varies from 0.5 to 0.8: $p = 2$ (———),
$p = 1$ (- - -), $p = 0$ (· · ·); $a/d = 0.5$ (□), 0.6 (*), 0.7 (×), 0.8 (+).

cylinders are separated. This provides us with the most compact way of illustrating the influence of near-trapping for any geometry consisting of N cylinders in a circular array. For example in Fig. 8, it can be seen how the peak in Linton and Evans [14] is due to the real-valued κa passing 'close' to the pole in the complex plane at approximately $1.67 - 0.11i$ and, as a/d is increased to 0.8, this pole moves to within 0.001 of the real line. Furthermore, the mode corresponds to $p = 2$ ($= N/2$). Thus, in the plots of maximum force against κa presented in Figs 2a–e, the peak in the forces can be associated with the occurrence of a pole in the complex plane close to the real axis. Clearly, as the pole moves closer to the real axis, one would expect the response in the forced problem to increase. We are also able to use Fig. 8 to identify the types of modes responsible for the peaks in the forces, and these are represented in Figs 2–4 by the circled values next to each of the peaks.

Figures 9 and 10 show the free-surface elevations Re{ϕ} and |ϕ| at the closest real values of κa for $a/d = 0.5$ and $a/d = 0.8$, respectively. Even in the case of

$a/d = 0.5$, corresponding to the relatively small peak in Fig. 2a, we see that the maximum elevation is some 3.5 times that of the incident wave. It can be seen that the maximum wave amplitude for the $a/d = 0.8$ near-trapped case is predicted to be over 150 times the incident wave amplitude and is responsible for the peak in the first-order force of 54 times that on an isolated cylinder. The motion in between the cylinders resembles a floppy saddle: where there is a wave peak on one cylinder, there is a trough on a neighbouring cylinder. From Fig. 8 we see that this mode is associated with a value $p = 2$ and this ties in with the prediction made by the analysis earlier for a $p = N/2$ mode where the force alternates in sign from one cylinder to the next.

The only other pole in the complex plane that comes near to the real line is the $p = 0$ mode as the cylinders are moved close together. Again, the free-surface plot in Fig. 11 shows that this rather weak near-trapped mode contributes to a tangential force on the array as predicted by the theory. Note that in order to excite this mode we would need to use an incident wave that destroys the geometric symmetric of the array and we have chosen $\theta_{\text{inc}} = 12.25°$ in Fig. 11
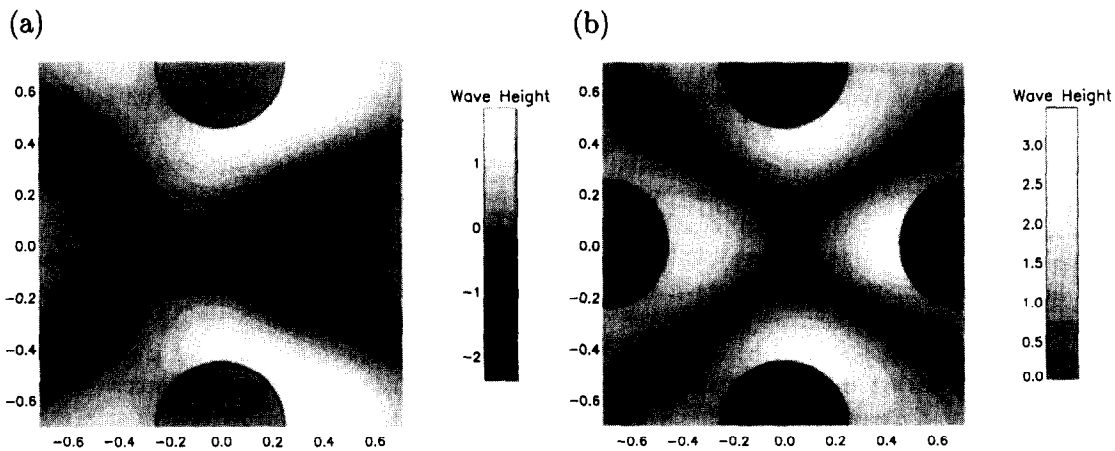

Fig. 9. (a) Re{ϕ} and (b) |ϕ| for $N = 4$, $a/d = 0.5$, $\kappa a = 1.66$, $\theta_{\text{inc}} = 0°$.
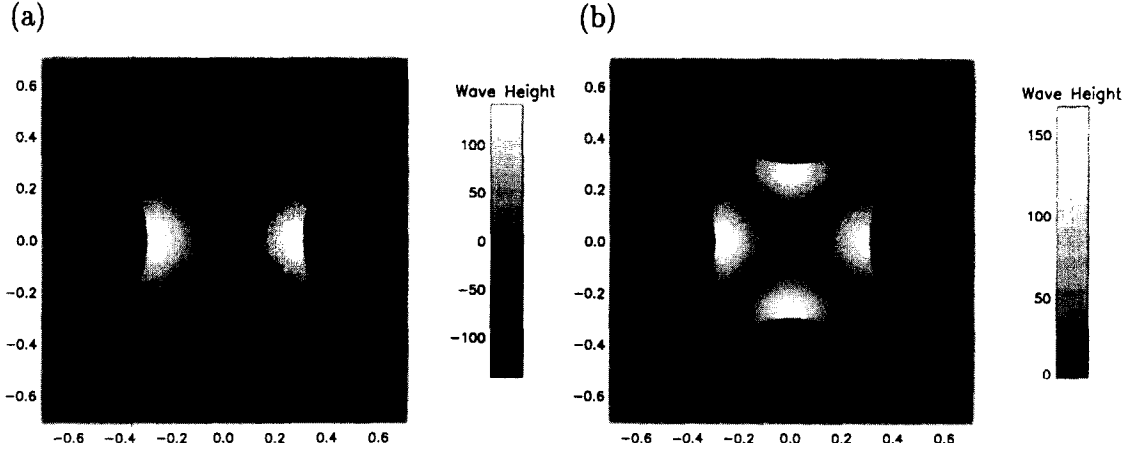
(a)   (b)

Fig. 10. (a) Re$\{\phi\}$ and (b) $|\phi|$ for $N = 4$, $a/d = 0.8$, $\kappa a = 4.08482$, $\theta_{\text{inc}} = 0°$.

(there is nothing special about this value). However, in Fig. 2a–e an incident wave with $\theta_{\text{inc}} = 0$ was used which preserved the symmetry and so no peaks corresponding to this $p = 0$ mode are observed.

We now consider the case of five cylinders, where it is not possible to generate a $p = N/2$ mode. In order to identify the near-trapped modes in this case, we again look at the poles of the determinant system in terms of complex κa. Fig. 12 shows the path of the poles for $p = 0$, 1 and 2 as a/d varies between 0.5 and 0.8 as in the previous case of $N = 4$. It can be seen from Fig. 12 that, for the spacing $a/d = 0.8$, there are three poles in the vicinity of the real line denoted by (+); two associated with the mode $p = 0$ and one with $p = 1$. Moreover, one of the $p = 0$ modes runs roughly parallel to the real line over the range of spacings $0.5 < a/d < 0.8$, whilst the poles associated with the remaining two modes will only have an influence on the forced problem as a/d approaches 0.8. The $p = 1$ mode eventually gets closest and is responsible for the maximum peak of 22 in the force plot in Fig. 3f. Figures 13–15 show the free surface excited by this particular near-trapped mode for three different incident wave angles: $\theta_{\text{inc}} = 0°$, 9° and 18°. The reason for choosing

three incident angles and not just $\theta_{\text{inc}} = 0$ is to illustrate the motion induced by a $p = 1$ mode. It can be seen that a single line of symmetry is sought (which depends on the incident angle) about which the fluid moves in an antisymmetric fashion. This is not apparent in the $\theta_{\text{inc}} = 0°$ case, which forces an additional even symmetry. The $p = 0$ mode corresponding to the pole running roughly parallel to the real axis in Fig. 12 can be seen in Fig. 3a–f to have an effect on the forces over the whole range of a/d from 0.4 to 0.8, with a maximum force on all cylinders in the array of approximately seven times the force on an isolated cylinder at $a/d = 0.6$. The free surface for $a/d = 0.8$ in this case is illustrated in Fig. 16 and it can be seen that the motion on all cylinders is the same and in phase, corresponding to the $p = 0$ mode predicted by the theory and illustrated in Fig. 7(b)(i). Thus, we expect an equal radial force on all cylinders in this mode and this is confirmed by Fig. 3a–f.

The remaining $p = 0$ mode corresponds to the motion depicted in Fig. 7(b)(ii) and the free surface elevation for $a/d = 0.8$ is shown in Fig. 17 where $\theta_{\text{inc}} = 0$. This motion gives us the peaks in the forces on all cylinders of
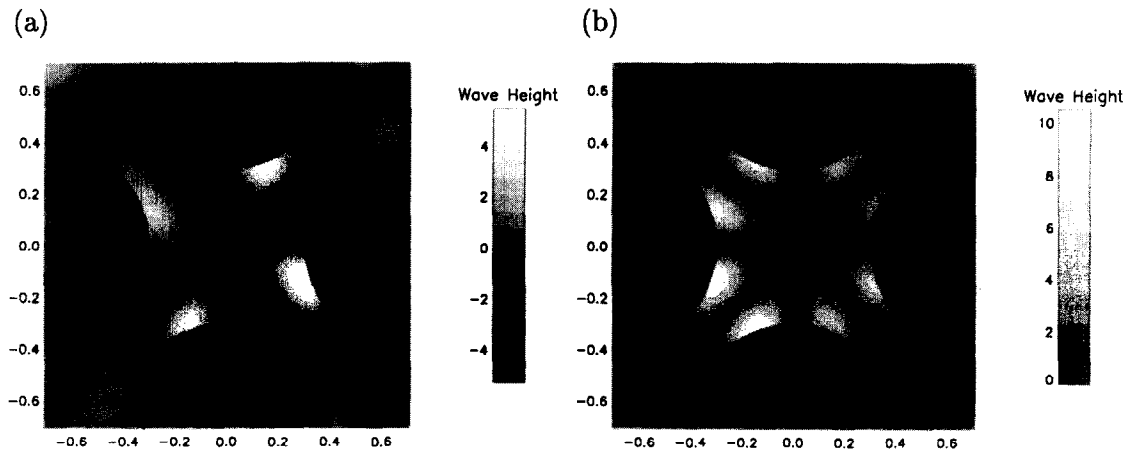
(a)   (b)

Fig. 11. (a) Re$\{\phi\}$ and (b) $|\phi|$ for $N = 4$, $a/d = 0.8$, $\kappa a = 5.797$, $\theta_{\text{inc}} = 12.25°$.
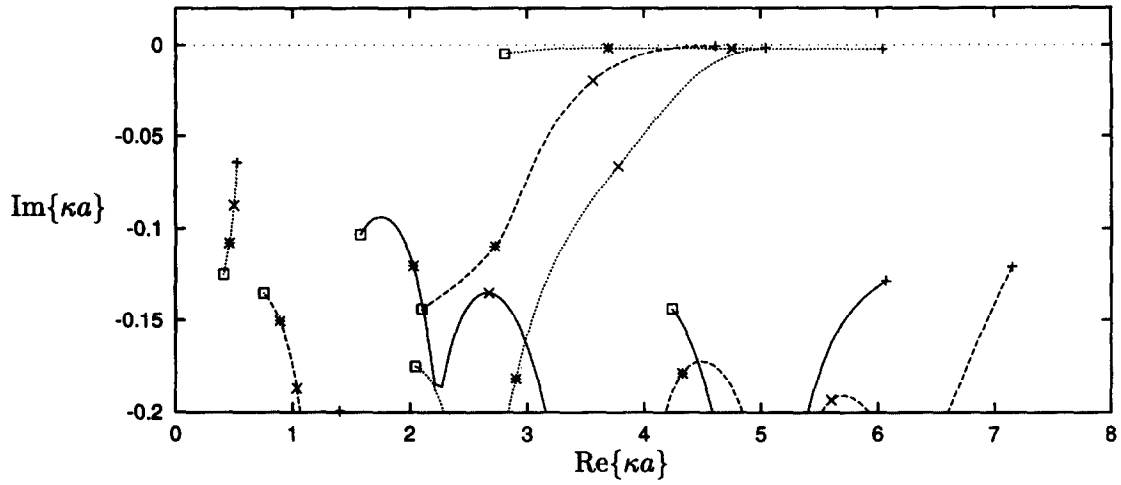
Fig. 12. Location of zeros of determinant in complex wavenumber κa space for $N = 5$ cylinders as a/d varies from 0.5 to 0.8: $p = 2$ (——),
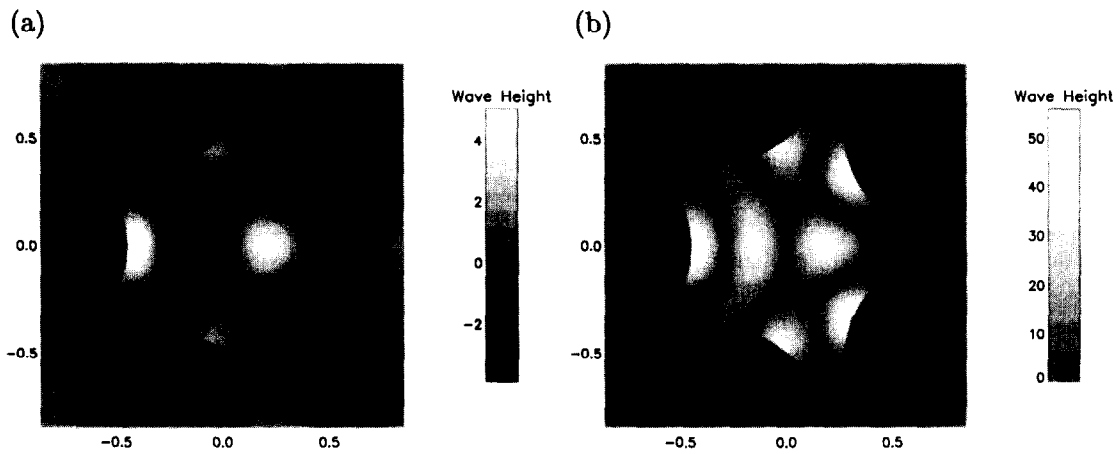$p = 1$ (- - -), $p = 0$ (· · ·); $a/d = 0.5$ ($\Box$), 0.6 (*), 0.7 ($\times$), 0.8 (+).

(a)   **(b)**

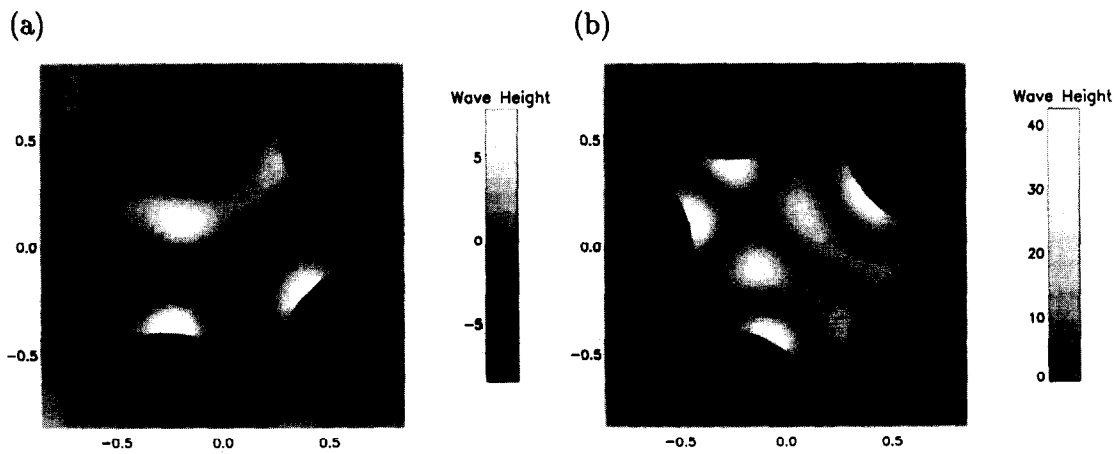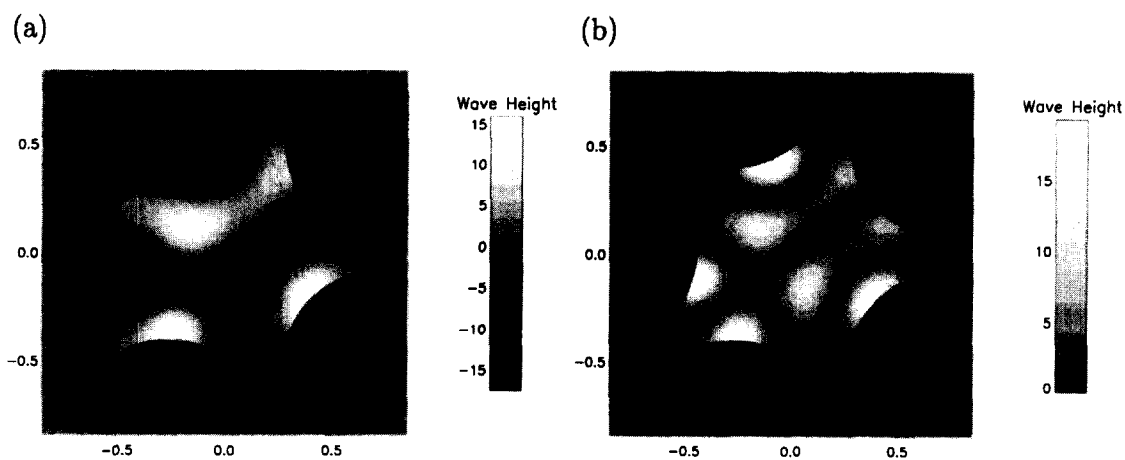**Fig. 13.** (a) Re$\{\phi\}$ and (b) $|\phi|$ for $N = 5$, $a/d = 0.8$, $\kappa a = 4.61048$, $\theta_{\text{inc}} = 0°$.

(a)   **(b)**

Fig. 14. (a) Re$\{\phi\}$ and (b) $|\phi|$ for $N = 5$, $a/d = 0.8$, $\kappa a = 4.61048$, $\theta_{\text{inc}} = 9°$.

(a) (b)

Fig. 15. (a) Re$\{\phi\}$ and (b) $|\phi|$ for $N = 5$, $a/d = 0.8$, $\kappa a = 4.61048$, $\theta_{\rm inc} = 18°$.

(a) (b)
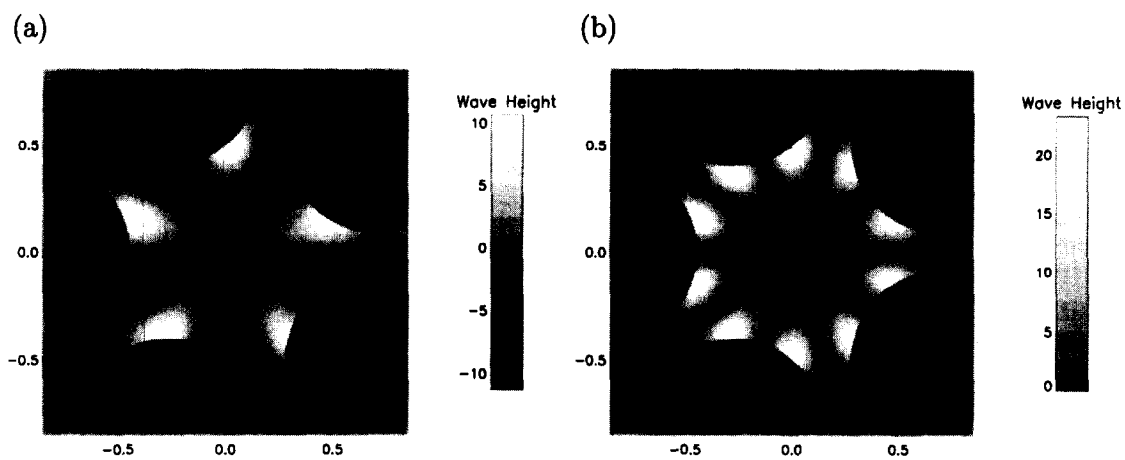
Fig. 16. (a) Re$\{\phi\}$ and (b) $|\phi|$ for $N = 5$, $a/d = 0.8$, $\kappa a = 5.0413$, $\theta_{\rm inc} = 18°$.
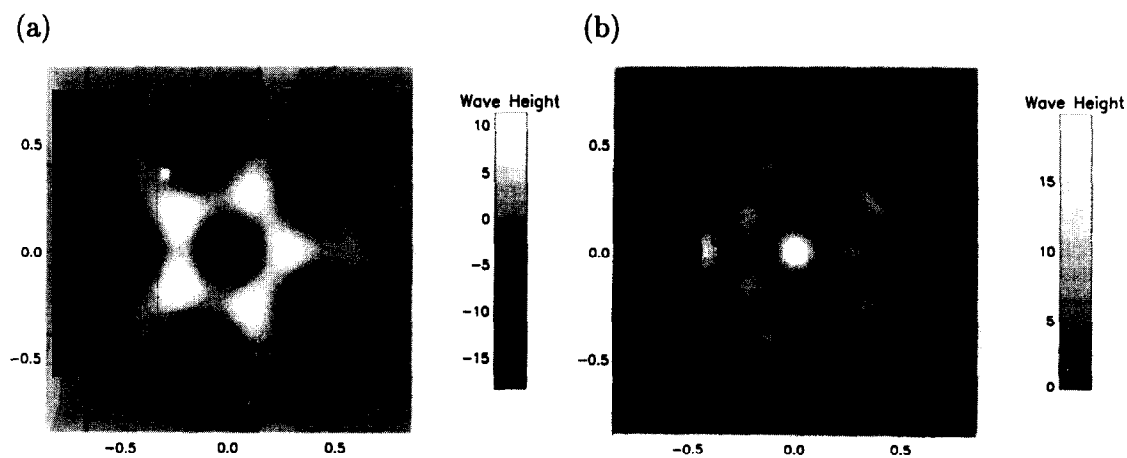
(a) (b)

Fig. 17. (a) Re$\{\phi\}$ and (b) $|\phi|$ for $N = 5$, $a/d = 0.8$, $\kappa a = 6.0413$, $\theta_{\rm inc} = 0°$.
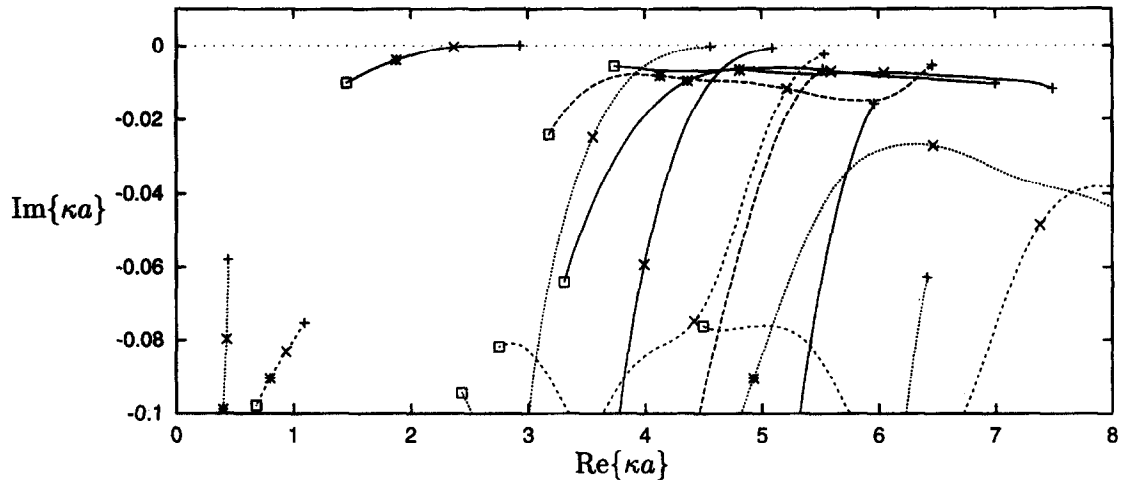
Fig. 18. Location of zeros of determinant in complex wavenumber κa space for $N = 6$ cylinders as a/d varies from 0.5 to 0.8: $p = 3$ (———),
$p = 2$ (— — —), $p = 1$ (- - -), $p = 0$ (· · ·); $a/d = 0.5$ (□), 0.6 (∗), 0.7 (×), 0.8 (+).

approximately five times the isolated cylinder force at this spacing and with $\kappa a = 6.0413$ in Fig. 3f.

The last case we look at in detail is six cylinders in a circular arrangement. Even with this small number of cylinders, the picture starts to get very complicated. As before, we track the poles of the complex determinant as a/d varies in Fig. 18 to identify the type of mode associated with the peaks in the forces in Fig. 4a–d in which the values of p are circled next to the corresponding peaks. The dominant mode in terms of generating large forces on the structure is the $p = N/2 = 3$ mode that has a pole at $\kappa a = 2.92921 - 0.000001i$ in the complex plane at a spacing of $a/d = 0.8$. This is responsible for the first-order exciting force of 225 on all six cylinders shown in Fig. 4d. In Fig. 19 it can be seen that the corresponding fluid motion is equivalent to the standing or 'saddle' mode seen in the case of four cylinders with $p = N/2$. There is another $p = N/2$ mode that becomes important as a/d increases beyond 0.7, creating a force of over eight times that on an isolated cylinder at $\kappa a = 5.085$ when $a/d = 0.8$

(see Fig. 4d). From Fig. 20 this can be seen to represent a more complicated standing mode type motion with the phase and hence forces alternating in sign from one cylinder to the next as expected from the theory of Section 2. As in the previous cases with arrays of four and five cylinders, there is a $p = 0$ mode which induces moderately large tangential loads on the array in the presence of an incident wave field that breaks the symmetry of the problem. Thus, for $a/d = 0.8$, $\theta_{inc} = 15°$ and at $\kappa a = 4.5582$, we see in Fig. 21 the same $p = 0$ standing mode already seen in Figs 11, and 16 for four and five cylinders.

From Fig. 4b–d we see a rather small peak corresponding to the mode $p = 2$, the relative wave amplification of which is shown in Fig. 22 when $a/d = 0.8$, $\kappa a = 6.4617$ and $\theta_{inc} = 0$. Behind the intricate pattern is a symmetry of motion that has been confirmed for incident wave directions other than $\theta_{inc} = 0$. In much the same way as the $p = 1$ mode for five cylinders was seen to seek a single line of symmetry about which the fluid motion was antisymmetric, here the $p = 2$ mode attempts to induce a motion which has two perpendicular lines of symmetry.
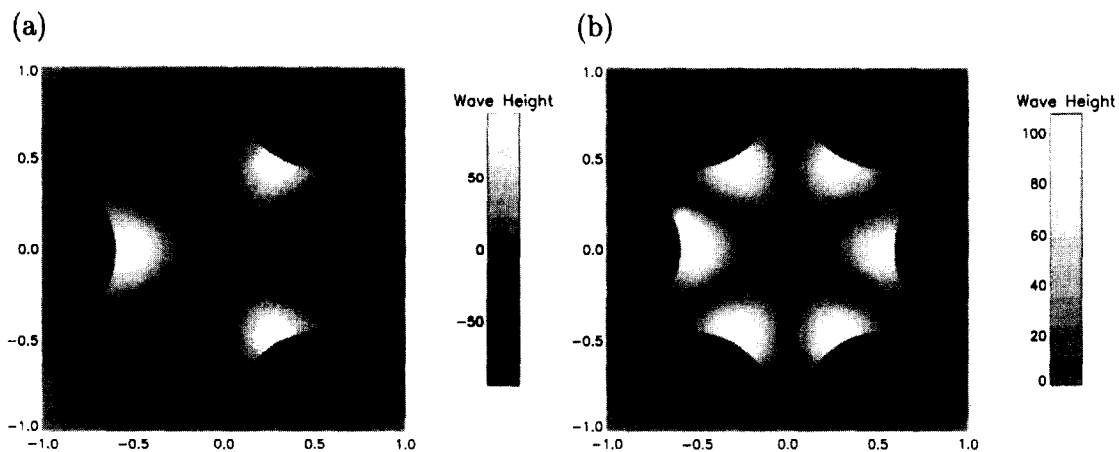
(a)   **(b)**

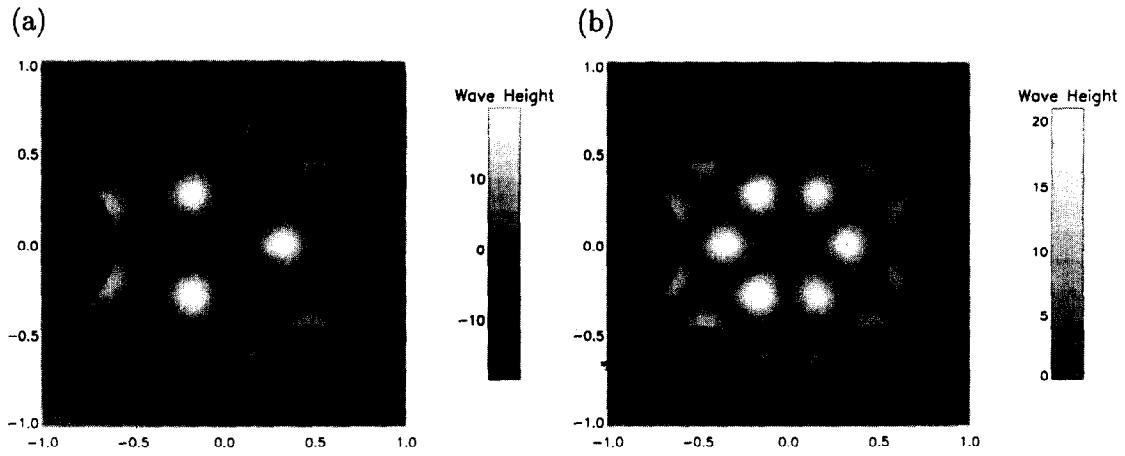**Fig. 19.** (a) Re$\{\phi\}$ and (b) $|\phi|$ for $N = 6$, $a/d = 0.8$, $\kappa a = 2.92922$, $\theta_{inc} = 0°$.

Fig. 20. (a) Re{ϕ} and (b) |ϕ| for $N = 6$, $a/d = 0.8$, $\kappa a = 5.085$, $\theta_{inc} = 0°$.

Fig. 21. (a) Re{ϕ} and (b) |ϕ| for $N = 6$, $a/d = 0.8$, $\kappa a = 4.5582$, $\theta_{inc} = 15°$.
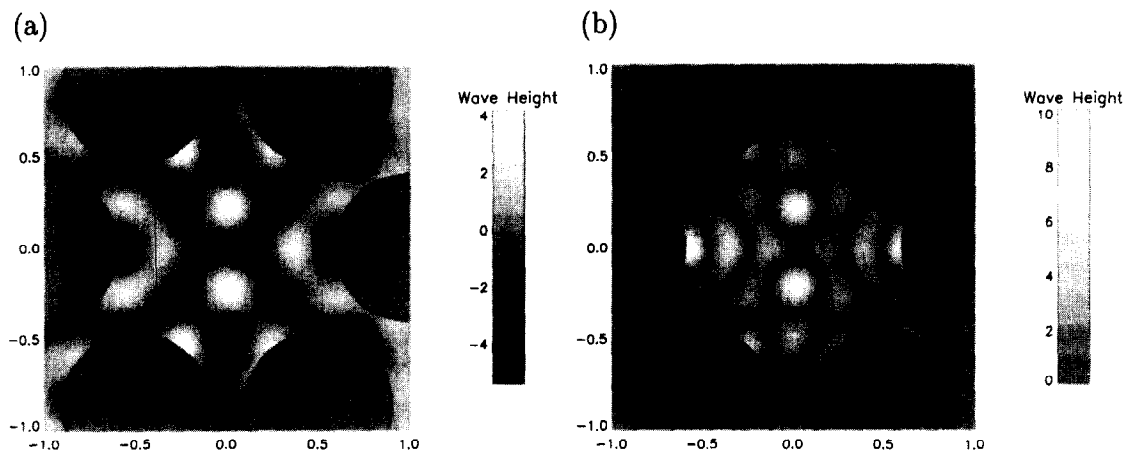
Fig. 22. (a) Re{ϕ} and (b) |ϕ| for $N = 6$, $a/d = 0.8$, $\kappa a = 6.4617$, $\theta_{inc} = 0°$.

Fig. 23. (a) $\mathrm{Re}\{\phi\}$ and (b) $|\phi|$ for $N = 6$, $a/d = 0.8$, $\kappa a = 5.5321$, $\theta_{\mathrm{inc}} = 0°$.
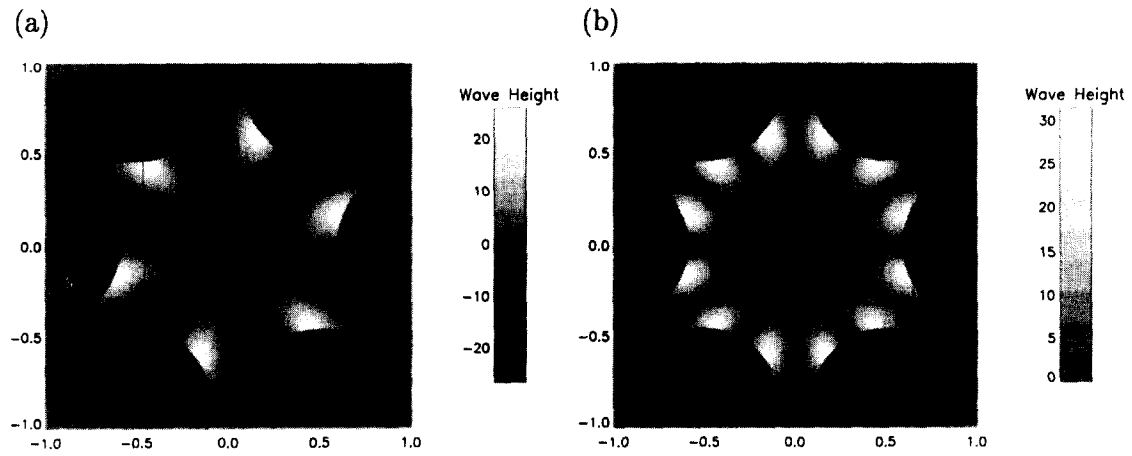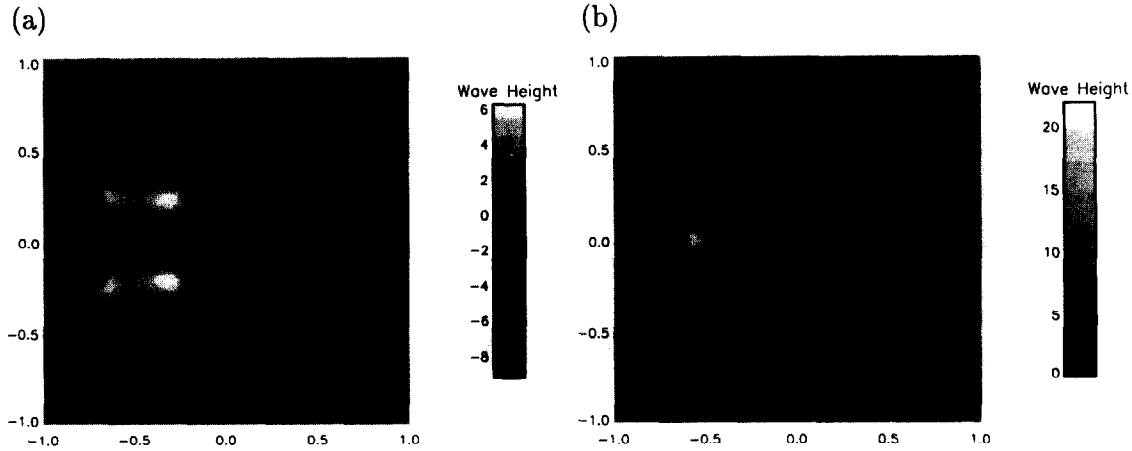
In the final plot for six cylinders in Fig. 23 we have sketched the free surface corresponding to the peak in the force in Fig. 4d at $\kappa a = 5.5321$ when $a/d = 0.8$. This mode is difficult to interpret since it arises as a consequence of the compound effects of two poles of the complex determinant close to the real axis corresponding to the values $p = 1$ and $p = 2$.

4 CONCLUSION

In this paper we have considered the effect of incident waves on arrays of identical, bottom-mounted, circular cylinders arranged in a circle. The method uses the interaction theory of Linton and Evans [4] to reduce the problem to the solution of an infinite system of equations for the Fourier coefficients in the expansion of the potential near any given cylinder. Particular attention was paid to circular arrays of four, five and six cylinders where it was shown that near-trapping and corresponding large forces and water displacements occur as the spacing between adjacent cylinders reduces. An understanding of this was gained through computation of the complex roots of the determinant of the system and by introducing an integer p related to the phase change in the potential in going from one cylinder to the next. Thus different values of p relate to different symmetries of the array.

It is possible, and for certain purposes desirable, to consider the circular array problem *ab initio* by using symmetry arguments. Thus the N-cylinder circular array is invariant under the symmetry group C_{Nv} and the general potential near each cylinder can be written in terms of a decomposition over the irreducible representations of C_{Nv}; see, for example, McWeeney [17]. By using these representations in eqn (A.16), separate infinite systems can be obtained for each of the representations and the zeros of the corresponding determinants in each case would correspond to near-trapping. Such an approach was used by Gaspard and Rice [16] in studying the scattering by three discs on each of which a Dirichlet boundary condition is satisfied.

The approach used here, to relate the Fourier coefficients at each cylinder through a value of p in eqn (A.24), was motivated by the work of Maniar and Newman [8] on the linear array and it has been shown that the peaks in the forces on circular arrays of four, five and six cylinders can in all cases be associated with a particular value of p. Generally speaking, for N even, solutions for $p = 0$ (or N) and $p = N/2$ produce the largest forces and water motion, and correspond to standing wave motions which were seen in the linear array to cause the large peaks in the forces, whilst for N odd $p = 0$ and 1 appear to be the most important.

Computations have been made on larger numbers of cylinders in a circular array and the structure of the possible solutions rapidly becomes very complex. In contexts other than in the offshore industry $N > 6$ is of greater interest, and more work needs to be done in understanding the large forces that can occur in such solutions owing to near-trapping.

ACKNOWLEDGEMENTS

APPENDIX A INTERACTION THEORY FOR AN ARBITRARY ARRAY OF CYLINDERS

The formulation follows that of Linton and Evans [4], see Fig. 24 for coordinate system, where the velocity potential Φ is expressed as

$$\Phi(x, y, z, t) = \mathrm{Re}\{\phi(x, y) \cosh \kappa(z + h)\, e^{-i\omega t}\} \qquad (A1)$$

where $\omega/2\pi$ is the wave frequency, h the depth of water and κ is the positive root of

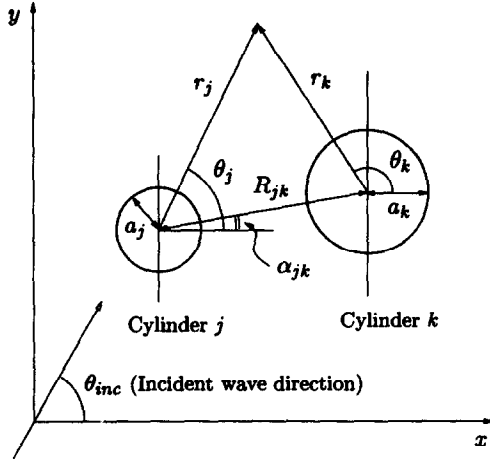$$\omega^2 = g\kappa \tanh \kappa h \qquad (A2)$$

Fig. 24. The coordinate system of Linton and Evans [14].

Then ϕ satisfies

$$\left(\nabla^2 + \kappa^2\right)\phi(x, y) = 0 \tag{A3}$$

exterior to the cylinders and

$$\frac{\partial\phi}{\partial n} = 0 \tag{A4}$$

on each cylinder.

We assume there are N circular cylinders having arbitrary position and radius and write

$$\phi(x, y) = \phi_{\text{inc}}(x, y) + \sum_{j=1}^{N} \phi_s^j(x, y) \tag{A5}$$

where

$$\phi_{\text{inc}}(x, y) = e^{i\kappa r \cos(\theta - \theta_{\text{inc}})} = I_k\, e^{i\kappa r_k \cos(\theta_k - \theta_{\text{inc}})} \tag{A6}$$

and

$$I_k = e^{i(x_k \cos\theta_{\text{inc}} + y_k \sin\theta_{\text{inc}})} \tag{A7}$$

Thus the incident wave makes an angle θ_{inc} with the x-direction and cylinder k has centre (x_k, y_k). The general form for the scattered potential from cylinder j is

$$\phi_s^j = \sum_{n=-\infty}^{\infty} A_n^j Z_n^j H_n\left(\kappa r_j\right) e^{in\theta_j} \tag{A8}$$

where

$$Z_n^j = J_n'\left(\kappa a_j\right)/H_n'\left(\kappa a_j\right) \tag{A9}$$

and a_j is the radius of cylinder j. Here $H_n \equiv J_n + iY_n$ is the Hankel function of the first kind. By using Graf's addition formula, Linton and Evans [4] showed that to satisfy eqn (A.4) then the coefficients A_m^k must satisfy

$$A_m^k + \sum_{\substack{j=1\\ \neq k}}^{N} \sum_{n=-\infty}^{\infty} A_n^j Z_n^j\, e^{i(n-m)\alpha_{jk}} H_{n-m}\left(kR_{jk}\right)$$

$$= -I_k\, e^{im(\pi/2 - \theta_{\text{inc}})}$$

$$\text{for } k = 1, \ldots, N, \quad -\infty < m < \infty \tag{A10}$$

Here, R_{jk} is the distance between the centres of cylinders j

and k, and α_{jk} is the angle between the line from the centre of cylinder j to the centre of cylinder k and the positive x-direction. Notice that the effect of the incident wave is included through the term θ_{inc} on the right-hand side.

It was shown in Linton and Evans [4] that the total potential may be expressed in the coordinates of cylinder j, say, as simply

$$\phi\left(r_j, \theta_j\right) = \sum_{n=-\infty}^{\infty} A_n^j F_n\left(\kappa r_j\right) e^{in\theta_j}, \quad r_j < R_{jk}\ \forall k \tag{A11}$$

where

$$F_n\left(\kappa r_j\right) = Z_n^j H_n\left(\kappa r_j\right) - J_n\left(\kappa r_j\right) \tag{A12}$$

and where r_j, θ_j are polar coordinates measured from the centre of cylinder j in the positive x-direction. From the above equation, the first-order exciting force on the jth cylinder can be derived. Thus

$$\frac{X^j}{F^j} = -\frac{1}{2}\left\{\begin{array}{c} i \\ 1 \end{array}\right\}\left(A_{-1}^j\left\{\begin{array}{c} - \\ + \end{array}\right\}A_1^j\right) \tag{A13}$$

where F^j is the first-order exciting force on a isolated cylinder, radius a_j, in the direction of the incident wave and the upper (lower) elements refer to the force in the x- (y-) direction.

The above derivation is entirely general and has been included for completeness. We now assume that the N cylinders are identical ($a_j = a, j = 1, \ldots, N$) and are equally spaced around a circle of radius R. It is convenient to exploit the symmetry of the cylindrical array and choose local polar coordinates at each cylinder measured from the line joining the centre of that cylinder to the centre of the array as shown in Fig. 25. It follows by elementary geometry that

$$\alpha_{jk} = \frac{\pi}{N}(k+j) + \frac{\pi}{2}\,\text{sgn}(k-j) \tag{A14}$$

where we have chosen cylinder j to make an angle of $2\pi j/N$ with the positive x-direction ($j = 1, 2, \ldots, N$) and to have its centre at

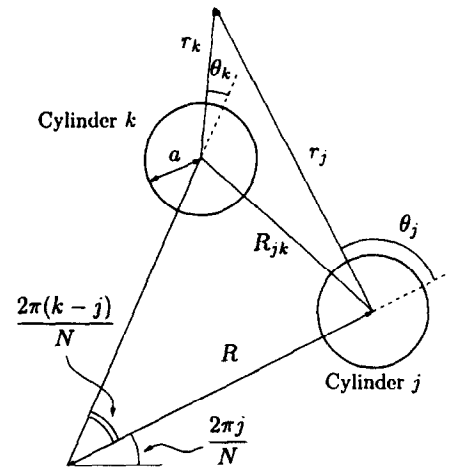$$x_j = R\cos(2\pi j/N), \quad y_j = R\sin(2\pi j/N) \tag{A15}$$

Fig. 25. The coordinate system for the cylindrical array.

Substitution of eqns (A.14), (A.15) into eqn (A.10) gives

$$B_m^k + \sum_{\substack{j=1 \\ \neq k}}^{N} \sum_{n=-\infty}^{\infty} B_n^j Z_n^j H_{n-m}(\kappa R_{jk})$$

$$\times \; e^{i\frac{1}{2}(n-m)\pi \; \mathrm{sgn}(k-j)} \; e^{i(n+m)\pi(k-j)/N}$$

$$= -I_k \, e^{im(\pi/2 + 2\pi k/N - \theta_{\mathrm{inc}})}$$

for $k = 1, \ldots, N$, $-\infty < m < \infty$ (A16)

where now

$$I_k = e^{i\kappa R \, \cos(2\pi k/N - \theta_{\mathrm{inc}})}$$ (A17)

from eqns (A.7), (A.15) and

$$R_{jk} = 2R \left| \sin \frac{\pi(k-j)}{N} \right|$$ (A18)

and we have also written

$$A_n^k \, e^{2\pi k n i/N} = B_n^k$$ (A19)

Note that the same result can be obtained by using local polar coordinates from the outset in eqn (A.8) with A_n^j replaced by B_n^j.

It is easily shown that the forces in the radial/tangential directions are

$$\frac{1}{F}\left\{ \begin{array}{c} X_j^r \\ X_\theta^j \end{array} \right\} = -\frac{1}{2}\left\{ \begin{array}{c} i \\ 1 \end{array} \right\} \left(B_{-1}^j \left\{ \begin{array}{c} - \\ + \end{array} \right\} B_1^j \right)$$ (A20)

normalised with respect to the force on an isolated cylinder of radius a in the direction of the incident wave. Either eqns (A.10), and (A.13) or eqns (A.16), and (A.20) can be used to determine the forces on cylindrical arrays of circular cylinders and, as expected, they give identical results. In particular, they confirm the corrected results of Linton and Evans for the first-order exciting force on four cylinders [14].

We can also compute the mean second-order drift force defined to be

$$f^j = \alpha \int_0^{2\pi} \left\{ \frac{1}{\kappa^2} |\nabla\phi|^2 \Big|_{r_j=a} - |\phi|_{r_j=a}^2 \right\} e^{i n \theta_j} \, d\theta_j$$ (A21)

where

$$\sigma = \frac{1}{8}\rho g A^2 a \left(1 + \frac{2\kappa h}{\sinh 2\kappa h}\right)$$ (A22)

on cylinder j in either the x- or y-direction by using Linton and Evans' eqn (3.8) [4] or in radial/tangential directions by substituting eqn (A.19) in the former equation [using appropriate local coordinates (r_j, θ_j)] to give

$$f^j = f_r^j + i f_\theta^j = \frac{8\alpha \, e^{2\pi j i/N}}{\pi(\kappa a)^2} \sum_{n=0}^{\infty} \left(\frac{n(n+1)}{(\kappa a)^2} - 1\right)$$

$$\times \left(\frac{B_{n+1}^{j*} B_n^j}{H_{n+1}^{'*}(\kappa a) H_n^{'}(\kappa a)} - \frac{B_{-n}^{j*} B_{-n-1}^j}{H_n^{'*}(\kappa a) H_{n+1}^{'}(\kappa a)} \right)$$ (A23)

where $*$ denotes complex conjugate. This is non-dimensionalised by the mean second-order drift force on a cylinder in isolation, resolved in radial/tangential directions,

$$f_1^j = f_{1r}^j + i f_{1\theta}^j = \frac{32\alpha}{\pi^2(\kappa a)^3} e^{2\pi j i/N} \sum_{n=0}^{\infty} \left(\frac{n(n+1)}{(\kappa a)^2} - 1\right)$$

$$\times \frac{1}{|H_n^{'}(\kappa a)|^2 |H_{n+1}^{'}(\kappa a)|^2}$$

see, for example, Linton and Evans [4], eqn (3.10).

Following the approach of Maniar and Newman [8] for the linear array, we shall seek near-trapped modes directly from eqn (A.16) by putting the right-hand side equal to zero and assuming a relationship between the B_n^k. Thus it might be expected that, for a near-trapped mode, B_n^k would differ from B_n^j only by a phase factor reflecting the angle $2\pi(k - j)/N$ between the cylinders. More generally, whilst preserving single-valuedness we may write

$$B_n^k = e^{i(k-j)2\pi p/N} B_n^j, \qquad \begin{array}{l} p \text{ an integer} \\ \\ j, k = 1, \ldots, N \end{array}$$ (A24)

whence substitution into eqn (A.16) gives

$$B_m^0 + \sum_{n=-\infty}^{\infty} B_n^0 K_{mn} = 0$$ (A25)

where the superscript zero indicates a cylinder in the 'zeroth' position on the positive x-axis. Here

$$K_{mn} = Z_n^0 \sum_{\substack{j=k-1 \\ \neq 0}}^{k-N} H_{n-m}\left(2\kappa R \sin\frac{\pi|j|}{N}\right) e^{2\pi p j i/N}$$

$$\times \, e^{i\frac{1}{2}(N-m)\pi \, \mathrm{sgn}(j)} \, e^{i(m+n)\pi j/N}$$ (A26)

after redefining the summation variable. This is easily seen to be independent of k by showing, in an obvious notation, that

$$K_{mn}(k) = K_{mn}(k+1), \quad k = 1, 2, \ldots, N$$ (A27)

It follows that in particular we may choose $k = N$, in which case K_{mn} reduces to

$$K_{mn} = Z_n^0 \, e^{i(n-m)\pi/2}$$

$$\times \sum_{j=1}^{N-1} H_{n-m}\left(2\kappa R \sin\frac{\pi j}{N}\right) e^{i(m+n-2p)\pi j/N}$$ (A28)

and we have reduced eqn (A.16) to the single infinite system, eqn (A.25), with K_{mn} as above.

REFERENCES

1. Twersky, V., Multiple scattering and radiation by an arbitrary configuration of parallel cylinders. *Journal of the Acoustic Society of America*, 1952, **24** 42–46.

2. Ohkusu, M., Hydrodynamic forces on multiple cylinders in waves. In *Proceedings of International Symposium on*

Dynamics of Marine Vehicles and Structures in Waves, London, 1974, Paper 12, pp. 107–112.

3. Spring, B.N. and Monkmeyer, P.L., Interaction of plane waves with vertical cylinders. In *Proceedings of 14th International Conference on Coastal Engineering*, 1974, pp. 1828–1845.

4. Linton, C.M. and Evans, D.V., The interaction of waves with arrays of vertical circular cylinders. *Journal of Fluid Mechanics*, 1990, **215** 549–569.

5. Huang, J.B. and Eatock-Taylor, R., Second-order interaction between waves and multiple bottom-mounted vertical circular cylinders. In *Proceedings of 11th International Workshop on Water Waves and Floating Bodies*, Hamburg, 1996.

6. Mavrakos, S.A. and Koumoutsakos, P., Hydrodynamic interaction among vertical axisymmetric bodies restrained in waves. *Applied Ocean Research*, 1987, **9** 128–140.

7. Kagemoto, H. and Yue, D.K.P., Interaction among multiple three-dimensional bodies in water waves: an exact algebraic method. *Journal of Fluid Mechanics*, 1986, **166** 189–209.

8. Maniar, H.D. and Newman, J.N., Wave diffraction by a long array of cylinders. *Journal of Fluid Mechanics*, 1997, **339** 309–330.

9. Callan, M., Linton, C.M. and Evans, D.V., Trapped modes in two-dimensional waveguides. *Journal of Fluid Mechanics*, 1991, **229** 51–64.

10. Ursell, F., Trapping modes in the theory of surface waves. *Proceedings of Cambridge Philosophical Society*, 1951, **47** 346–358.

11. Evans, D.V., Levitin, M. and Vassiliev, D., Existence theorems for trapped modes. *Journal of Fluid Mechanics*, 1994, **261** 21–31.

12. Davies, E.B. and Parnovski, L., Trapped modes in acoustic waveguides. *Quarterly Journal of Mechanics and Applied Mathematics*, in press.

13. Parker, R. and Stoneman, S.A.T., The excitation and consequences of acoustic resonances in enclosed fluid flow around solid bodies. *Proceedings of the Institution of Mechanical Engineers*, 1989, **203** 9–19.

14. Linton, C.M. and Evans, D.V., Corrigendum: The interaction of waves with arrays of vertical circular cylinders. *Journal of Fluid Mechanics*, 1990, **218** 663.

15. McIver, P. and Evans, D.V., Approximation of wave forces on cylinder arrays. *Applied Ocean Research*, 1984, **6**(2) 101–107.

16. Gaspard, P. and Rice, S.A., Exact quantization of the scattering from a classically chaotic repellor. *Journal of Chemical Physics*, 1989, **90**(4) 2255–2262.

17. McWeeney, R., Symmetry: An Introduction to Group Theory and its Applications. Pergamon Press, Oxford, 1963.